Research Article

On the Influences of Air Bubbles on Water Flow in a Two-Dimensional Channel

Wenyun Huang,[1,2,3] Honglu Yun,[4] Wenchao Huang,[1,2,3] Bin Zhang,[1,2,3] and Xujian Lyu [1D][4,5]

[1]*Fishery Machinery and Instrument Research Institute, Chinese Academy of Fishery Science, Shanghai 200092, China*
[2]*Key Laboratory of Ocean Fishing Vessel and Equipment, Ministry of Agriculture, Shanghai 200092, China*
[3]*Joint Laboratory for Open Sea Fishery Engineering, Pilot National Laboratory for Marine Science and Technology (Qingdao), Shandong, Qingdao 266237, China*
[4]*School of Energy and Power Engineering, Nanjing University of Science and Technology, Nanjing 210094, China*
[5]*State Key Laboratory of Ocean Engineering, Shanghai Jiao Tong University, Shanghai 200240, China*

Correspondence should be addressed to Xujian Lyu; xjlyu@njust.edu.cn

As an inevitable trend for the sustainable development of the global economy, saving energy and reducing emissions are key goals for the entire world. The use of air bubbles to reduce viscous friction is one of the most effective approaches to achieve this goal, as it may significantly reduce the frictional drag of ships. However, the injection of air bubbles will change flow characteristics near the wall due to the significant differences in density and viscosity between air and water. In addition, parameters such as bubble size, bubble surface tension, bubble number and bubble position also affect the flow near the wall, resulting in significant diversity and instability in two-phase flow. To clarify the mechanism of these effects, a two-dimensional channel flow with air bubbles is studied using Computational Fluid Dynamics (CFD). The interactions between bubbles and water and between bubbles and wall are studied, and the detailed characteristics of bubbles moving in fully developed flow are considered. This study shows that the velocity gradient is the main factor influencing wall shear stress, and the presence of bubbles has a marked impact on the local velocity gradient distribution of the nearby flow. It is also found that shorter distance between a bubble and the wall enhances the flow interaction and leads to more significant perturbations of wall shear stress.

1. Introduction

The use of air bubbles is one of the most effective approaches to reduce drag for ships. The interactions during air bubbles, water flow and ship walls play an important role in the application of such bubble drag-reduction technology. In this paper, the interaction mechanism of bubbles, water and wall surface in two-dimensional pipeline flow is studied, and its mechanism is analyzed by numerical simulation. Bubbles can reduce frictional drag of a moving body by changing the properties of the near-wall fluid flow [1–3]. The maritime shipping industry is thus interested in employing this drag-reduction technology to reduce energy use and greenhouse gas emissions [4, 5]. The use of bubbles to reduce skin frictional drag of ships' external turbulent flow is a long-term engineering goal [6, 7]. Although the industrial community mainly cares about drag-reduction effects for full-scale ships, understanding the mechanisms of complex water-bubble interactions and bubble-wall interactions is one of the key components for this goal [8]. It is generally acknowledged that drag reduction using bubbles depends on the properties of bubbly flows, such as bubbles' size, void fraction and their interactions with water [9].

Experimental study is one of the most important methods for the investigation of bubbly flow, due to its reliability and robustness. A series of studies have been carried out on drag reduction using bubbles, and the influence of injected bubble was analyzed [10–13]. Verschoof

et al. [14] found that bubble deformability was a fundamental factor of bubble drag reduction in turbulent flow. Rawat et al. [15] discussed the influence of micro-bubbles on turbulent flow, and they discovered that the bubble effect plays a major role in the improvement of flow structures. Shen et al. [16] experimentally revealed that drag reduction with bubbles was obviously related to the volumetric flow rate of injected gas and the static pressure of boundary layer.

However, the limited physical space and overlap of bubbles in mixed-regime flows make it difficult to observe the complicated but important bubble-water-wall interactions in experiments. Complementary to experimental study, numerical simulation is an important option, since it can provide valuable flow details that are challenging to measure experimentally. In addition, numerical simulation has been applied to various fields, including heat transfer and nanofluids [17–22]. Hence, a great deal of research has been carried out in the recent years through numerical simulations [23–26]. Xu et al. [27] discovered that a sustained level of drag reduction can be achieved by seeding small bubbles in a turbulent channel flow through direct numerical simulation. Pang et al. [28] numerically simulated the drag reduction through the use of small bubbles, and found rules for drag reduction according to the bubbles' size and the liquid-phase Reynolds number. Lu et al. [29, 30] used direct numerical simulations to model bubble deformation and drag reduction with bubbles, and found that bubble deformability usually resulted in different void fraction distributions. Lyu et al. [31] assessed the roles of several bubble parameters in the drag reduction for a SUBOFF submarine model, and found that the air injection velocity ratio and air volume fraction are critical for drag performance of the submarine. Marinho et al. [32] numerically studied the flow in curved ducts with Taylor bubbles using a commercial software package CFX, and discussed the transient effects of the air concentration on the volume fraction and viscosity of bubbly flows. Fox [33] reviewed the development of large-eddy-simulation tools for dispersed multiphase flows including use of bubbly flow for drag reduction. It is found that CFD modeling of bubbly flow still faces some significant challenges.

The prior studies in the area of drag reduction with air bubbles usually focused on bubbly flow with a mass of bubbles [34–36]. Bubble drag reduction is cumulative with the action of discrete bubbles, so that study focusing on the change in drag of a plate due to discrete air bubbles, that is, a single bubble or two bubbles, is essential. However, the experimental measurement and data analysis for application of discrete small bubbles are seldom implemented, due to the insufficient precision and great difficulty of controlling such small discrete bubbles. Furthermore, few investigations have been conducted to characterize discrete bubbles in the boundary layer using CFD methods as well. Therefore, a simple two-dimension CFD model coupled with the volume of fluid (VOF) method is applied to study the bubbles' effects on the flow characteristics and the wall shear stress in this paper. Several parameters including bubble size, bubble number, surface tension, and initial bubble position are taken into account to demonstrate the interesting bubbly flow.

2. Numerical Configuration

In this study, the ANSYS Fluent commercial software package is applied for two-dimension numerical simulation to study bubbly flow characteristics in a two-dimensional channel. A finite volume method is used to discretize computational domain and the VOF method is applied for bubble interface capture. The standard k-ε turbulence model is used to demonstrate turbulent flow near the channel's boundaries at the walls.

The equation for conservation of mass is given as

$$\frac{\partial (\rho u_i)}{\partial x_i} = 0, \tag{1}$$

The momentum equation is

$$\frac{\partial}{\partial t}\left(\rho u_i\right) + \frac{\partial}{\partial x_j}\left(\rho u_i u_j\right) = \frac{\partial}{\partial x_j}\left[\mu\left(\frac{\partial \mu_i}{\partial x_j} + \frac{\partial \mu_j}{\partial x_i}\right) - \frac{2}{3}\mu\frac{\partial \mu_i}{\partial x_j}\right]$$
$$- \frac{\partial P}{\partial x_i} + \rho g_i + F_i + \frac{\partial}{\partial x_j}\left(\overline{\rho \mu_i' \mu_j'}\right), \tag{2}$$

In these equations, u is the velocity, the subscripts i and j are 1 or 2 and represent x or y components, respectively, and μ is the viscosity of water.

The standard k-ε model is based on equations describing the turbulence kinetic energy k and turbulence dissipation rate ε. The transport equation for the turbulent kinetic energy k is [37]

$$\frac{\partial}{\partial t}\left(\rho k\right) + \frac{\partial}{\partial x_i}\left(\rho k u_i\right) = \frac{\partial}{\partial x_j}\left[\left(\mu + \frac{\mu_t}{\sigma_k}\right)\frac{\partial k}{\partial x_j}\right]$$
$$+ G_k + G_b - \rho\varepsilon - Y_M + S_k. \tag{3}$$

The transport equation for the turbulence dissipation rate ε is

$$\frac{\partial}{\partial t}\left(\rho\varepsilon\right) + \frac{\partial}{\partial x_i}\left(\rho\varepsilon u_i\right) = \frac{\partial}{\partial x_j}\left[\left(\mu + \frac{\mu_t}{\sigma_\varepsilon}\right)\frac{\partial k}{\partial x_j}\right]$$
$$+ C_{1\varepsilon}\frac{\varepsilon}{k}\left(G_k + C_{3\varepsilon}G_b\right) - C_{2\varepsilon}\rho\frac{\varepsilon^2}{k} + S_\varepsilon, \tag{4}$$

where G_b is the generation of turbulence kinetic energy due to buoyancy, Y_M is the contribution of the fluctuating dilatation in compressible turbulence to the overall dissipation rate, and $C_{1\varepsilon}$, $C_{2\varepsilon}$, and $C_{3\varepsilon}$ are constants. Parameters σ_k and σ_ε are the turbulent Prandtl numbers for k and ε, respectively. Terms S_k and S_ε are user-defined source terms, and the term G_k is the generation of turbulence kinetic energy due to the mean velocity gradients and can be defined as

$$G_k = -\rho \overline{u'_i u'_j} \frac{\partial u_j}{\partial x_i}. \tag{5}$$

The turbulent viscosity, μ_t, is determined by combining k and ε as follows:

$$\mu_t = \rho C_\mu \frac{k^2}{\varepsilon}, \tag{6}$$

where C_μ is a constant.

The VOF method implemented in Fluent uses a multidimensional universal limiter with an explicit solution algorithm. Together with an interface compression algorithm, this method ensures a sharp interface and limits the volume fraction α_q of the qth phase to values between 0 and 1. The momentum equation of the qth phase takes the following form

$$\frac{1}{\rho_q} \left[\frac{\partial}{\partial t} \left(\alpha_q \rho_q \right) + \nabla \cdot \left(\alpha_q \rho_q \overrightarrow{v}_q \right) = S_{\alpha_q} + \sum_{p=1}^{n} \left(\dot{m}_{pq} - \dot{m}_{qp} \right) \right], \tag{7}$$

where $\dot{m}_{qp}$ is the mass transfer from phase q to phase p and $\dot{m}_{pq}$ is the mass transfer from phase p to phase q. The continuum surface force model has been implemented so that the addition of surface tension to the VOF calculation results in a source term in the momentum equation. In this model, the surface tension is constant along the surface and where only the forces normal to the interface are considered. The pressure drop across the surface depends upon the surface tension coefficient, and the surface curvature is measured by two radii in orthogonal directions.

The ANSYS ICEM commercial software package is used for geometry modeling and mesh generation. The region of flow simulation, which is set to have a 10 mm height and 100 mm length, is discretized with uniform quadrilateral elements as shown in Figure 1. Boundary conditions including velocity inlet, wall, and outflow are used at the boundaries of the flow region, as shown in Figure 1. Mesh dependence and time-step dependence are studied, and a mesh number of 0.4 million (Figure 2) and time step of 10^{-5} s are verified to be adequate for this two-phase flow simulation. Transient numerical simulation is first conducted for the channel with 100 mm length until a fully developed two-dimension turbulent flow is achieved. The water flow simulation is conducted with parameters as follows: the water density is $\rho = 998.2$ kg/m^3, the dynamic viscosity is $\mu = 0.001003$ N·s/m^2, the flow velocity is $u = 0.5$ m/s, and the Reynolds number Re $= \rho u h / \mu = 4976$ is based on the channel height h. Typical velocity profiles at the end of every simulation period are presented in Figure 3(a), and the velocity profiles between the 3$^{\text{rd}}$ and 4$^{\text{th}}$ differs a little (Figure 3(b)). A more clear illustration of the velocity profiles for the 4$^{\text{th}}$ period is also shown in Figure 4 to further illustrate that the flow is fully developed at that time.

Experimental data for two parallel plates by Whan and Rothfus [38] are introduced to validate the present CFD framework, with comparison of velocity profiles at Reynolds numbers around 5000, as shown in Figure 5, where U_{max} is

the maximum of velocity along the x direction. With consideration of the differences of Reynolds numbers and the imperfection of present two-dimensional model, it is found that the results from CFD and experiment agree with each other in an acceptable degree. As a consequence, the CFD framework is applied in the subsequent simulations of bubbly flows.

3. Results and Discussion

To investigate the influence of air bubbles on two-phase flow characteristics, parameters including bubble size, surface tension, bubble number, and initial bubble position are taken into account during the simulation. Effects of those parameters on the wall shear stress at a certain monitoring point and frictional drag at the wall are monitored, as shown in Figure 6. The simulation cases and corresponding drag at the wall are listed in Table 1, and the condition descriptions for these cases are listed in Table 2.

It is well-known that friction at the wall is decided by wall shear stress, and the wall shear stress is described by the Law of Newton inner friction $\tau = \mu (dU_x/dy)$, in which μ is dynamic viscosity of the fluid, U_x is the local velocity along the tangential axis of the wall and y is the normal axis of the wall. To analyze the influence of the dynamic viscosity and velocity gradient on the wall shear stress, three typical time points in Case 9 are selected, as shown in Figure 7. The wall shear stress decreases rapidly after reaching a peak point ($t > 0.16$ s) and then increases quickly to another peak point. That is because the distance from the bubble to the wall dh is 0.5 mm in Case 9 and the bubble stays close to the wall, as the bubble approaches the monitoring point, the effects of bubbles on the flow distribution gradually increase, and the velocity gradients at time points a_1 and a_3 are bigger than those at other points. This makes the wall shear stress at time points a_1 and a_3 bigger than that without bubbles. As shown in Figure 8, the velocity gradients at time points a_1, a_2, and a_3 have little difference, while the wall shear stress at time point a_2 is much less than that of the other two time points. The reason for this phenomenon may be the fact that the bubble is right under the monitoring point; as a result the fluid viscosity is mainly decided by the air viscosity. In other words, the major factor affecting wall shear stress is the fluid viscosity when the bubble is close to the wall; the effect of the velocity gradient on the wall shear stress is very weak.

3.1. Effects of Bubble Size. Bubbles with different diameters, that is, 0.5 mm and 1 mm, are modeled to study the effects of bubble size on the wall shear stress at the monitoring point and drag at the wall, corresponding to Cases 1 and 2 as listed in Table 1. The initial distance from the bubble to the wall is set to 5 mm. It is found that larger bubble makes a little more perturbation on drag than the smaller bubble does, and both bubbles lead to a drag increase instead of reduction, as shown in Figures 9 and 10. At the earlier stage, the drag at the wall clearly starts to increase at time point b_1 for Case 1, and at time point b_2 for Case 2, respectively. Furthermore, an interesting phenomenon occurs that the drag curves
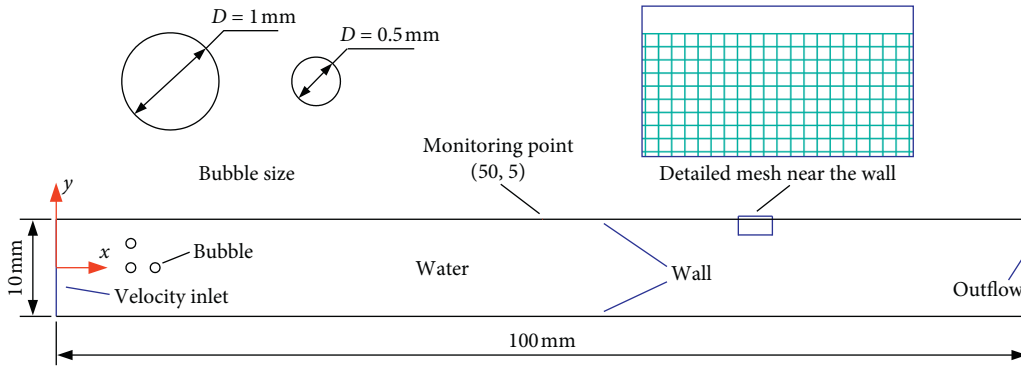
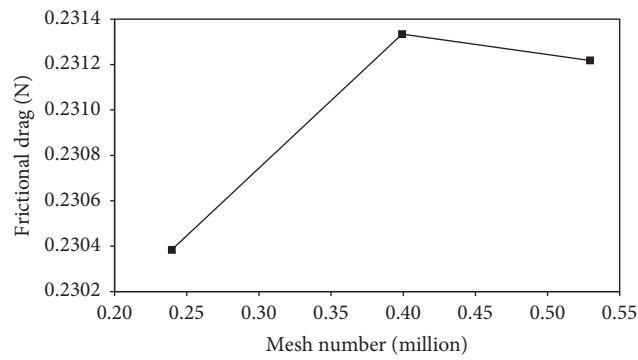FIGURE 1: Sketch of the two-dimension simulation model.
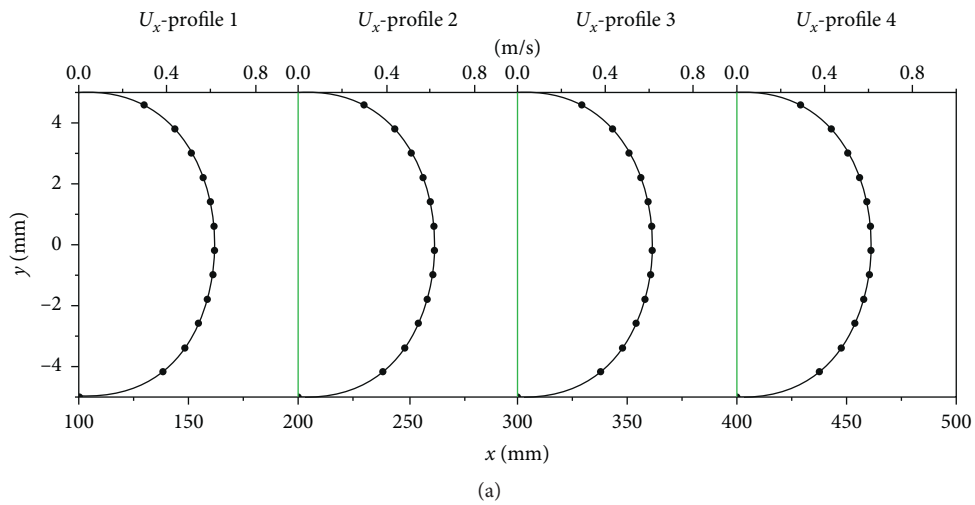

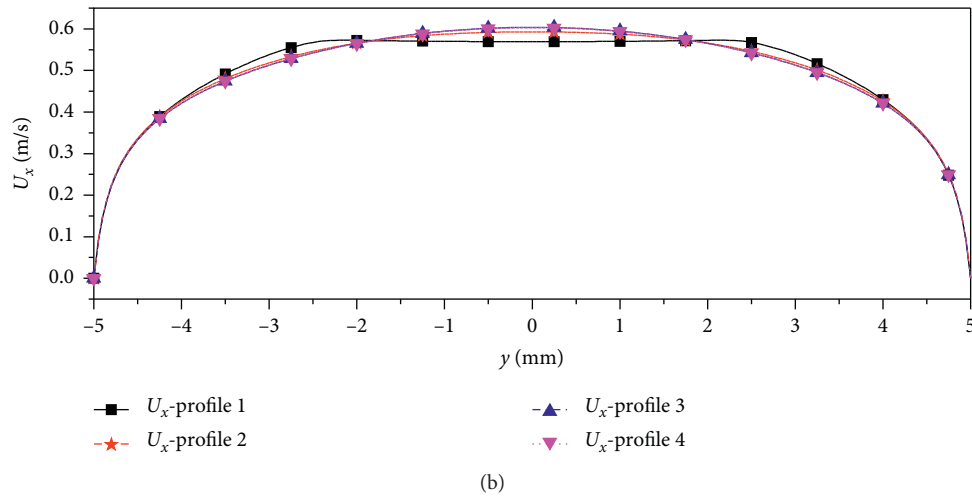FIGURE 2: Verification of mesh independence.

(a)

FIGURE 3: Continued.

(b)

FIGURE 3: Velocity profiles at the flow outlet after 4 time periods of simulation. (a) Detailed velocity profiles along the flow direction. (b) Development of the velocity profiles.
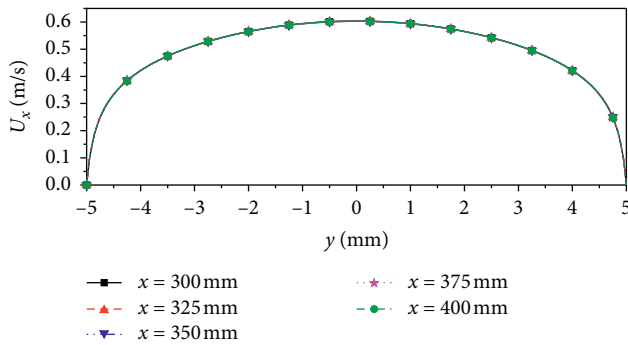

FIGURE 4: Velocity profiles almost overlap at different position along the flow direction of the 4th period flow simulation.
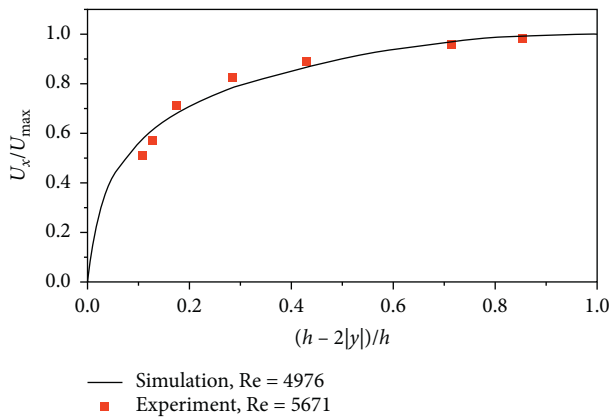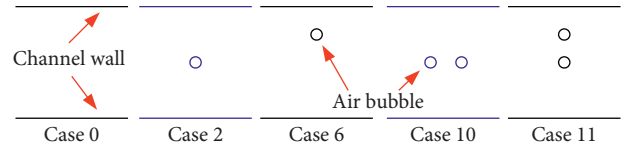

FIGURE 6: Sketch of the model for typical cases of the simulations presented.

not difficult to understand that a larger bubble takes more time and consequently results in different time delays for Cases 1 and 2. The velocity distribution and profiles near the monitoring point are shown in Figure 11. It is clear that velocity gradient of Case 2 is slightly bigger than that of Case 1. In addition, both the velocity contours and velocity profiles around the bubble at three different positions are shown in Figure 12. As the bubble moves along the channel, the velocity contour and velocity profiles at $x = 50$ mm change significantly compared to those at $x = 20$ mm, while they change little as the bubble moves from $x = 50$ mm to $x = 80$ mm as shown in Figure 12. This further proves that the two-phase flow is fully developed before it reaches the monitoring point ($x = 50$ mm).

FIGURE 5: Comparison of fully developed velocity profiles from experiment and present simulation.

3.2. Effects of Surface Tension. Surface tension usually plays a certain role in multiphase interface. Oishi and Murai [33] found that bubbles have rotating effects that engage with the two neighboring vortices to reduce drag at high Weber number, which is set as $We = \rho U^2 D/\sigma$, where σ is surface tension. To clarify such effect, some cases with different surface tensions, that is, 0.01, 0.072, and 0.15 (corresponding to Weber number varying from 1.67 to 24.96), are taken into account, as listed in Table 1. The bubble deformation ratio is defined as D_a/D_b, where D_a is the major diameter of the bubble and D_b is the minor diameter. It is found that the bubble achieves a significant deformation under a surface tension of $\sigma = 0.01$ N/m, while it deforms only a little under two other conditions of $\sigma = 0.0728$ N/m and 0.15 N/m, as shown in Figure 13. Furthermore, it is observed that surface

intersect at time point b_3, and the drag at the wall for Case 2 is larger than that for Case 1 after time point b_3 in Figure 9. When the bubble goes through the monitoring point at time point b_4, the drag at the wall shows little change. One possible reason for this phenomenon is that when the bubbles are introduced into the fully developed water flow with zero speed, it takes time for them to join the flow. It is

TABLE 1: Case list of the simulations.

Case	Bubbles number	Bubble size (mm)	Initial bubble position (mm)	Surface tension (N/m)	Frictional drag of the wall (N)
0	No bubble	—	—	—	0.231333
1	1	0.5	(5, 0)	0.0728	0.231525
2	1	1	(5, 0)	0.0728	0.231632
3	1	1	(5, 0)	0.01	0.231360
4	1	1	(5, 0)	0.15	0.231830
5	1	1	(5, 1.25)	0.0728	0.231655
6	1	1	(5, 2.5)	0.0728	0.231810
7	1	1	(5, 3)	0.0728	0.231940
8	1	1	(5, 3.5)	0.0728	0.232027
9	1	1	(5, 4.5)	0.0728	0.230971
10	2	1	(5, 0); (7.5, 0)	0.0728	0.232016
11	2	1	(5, 0); (5, 2.5)	0.0728	0.232060

TABLE 2: Conditions description for simulated cases.

Description	Effect of bubble size	Effect of surface tension	Effect of bubbles number	Effect of initial position of single bubble	Effect of initial arrangement of bubbles
	Case 0	Case 2		Case 2	
	Case 1	Case 3	Case 2	Case 5	Case 10
Case list	Case 2	Case 4	Case 10	Case 6	Case 11
				Case 7	
				Case 8	
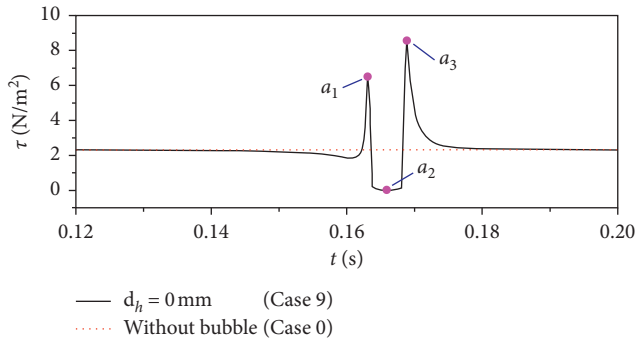
FIGURE 7: Effects of bubble size on shear stress at the channel wall.

tension has an important influence on wall shear stress at the monitoring point in Figure 14, and the wall shear stresses of Cases 2 and 4 are bigger than that of Case 3. The variation trend of drag at the wall accords with that of the wall shear stress, as shown in Table 1. In order to analyze the mechanism for this phenomenon, three typical time points (c_1, c_2, and c_3) are selected for further investigation, as shown in Figure 14. The velocity gradient at time point c_1 is bigger than that at other time points and the velocity at time point c_3 is the lowest one, as shown in Figure 15. The effects of bubbles on flow structure at the above three time points are shown in Figure 16. When the bubble just passes the monitoring point, the wall shear stress reaches its maximum value. Furthermore, the disturbance to the flow field is more significant under the surface tension of 0.15 than that of the other two cases. This effect is slightest for Case 3, which also confirms the variations of wall shear stresses at different time points. The reason for this phenomenon could be that the

interaction of a bubble and the fluid is neutralized by the bubble deformation for Case 3. To reveal more details, a variation of turbulent kinetic energy due to the change in surface tension is shown in Figure 17. The variation trend is similar to the wall shear stress at the monitoring point. With the comparison between cases of presence and absence of bubbles, it is found that the change of turbulent kinetic energy around the bubble is obvious for the surface tension of 0.15 but there is little change when the surface tension is 0.01.

3.3. Effects of Bubbles Number.

The effects of bubbles number on the wall shear stress at the monitoring point are depicted in Figure 18, corresponding to Cases 2 and 10 in Table 1. It is found that wall shear stress at the monitoring point increases with the increase of the number of bubbles. Due to the enhanced action with multiple bubbles, the peak value of the wall shear stress with two bubbles is more than twice the peak value with a single bubble, as shown in Figure 18. The wall shear stress achieves a peak value at about 0.005 s after bubbles pass the monitoring point. The wall shear stress variation is mainly influenced by the presence or absence of bubbles: they change the local flow structures. The velocity gradients near the monitoring point for Cases 2 and 10 have a similar tendency towards variation with the wall shear stress, as shown in Figure 19. As a result, drag at the wall for Case 10 is bigger than that for Case 2, as shown in Table 1.

3.4. Effects of the Initial Position of a Single Bubble.

To study the influence of initial bubble position on the change in drag at the wall within a bubbly flow, simulations on a single
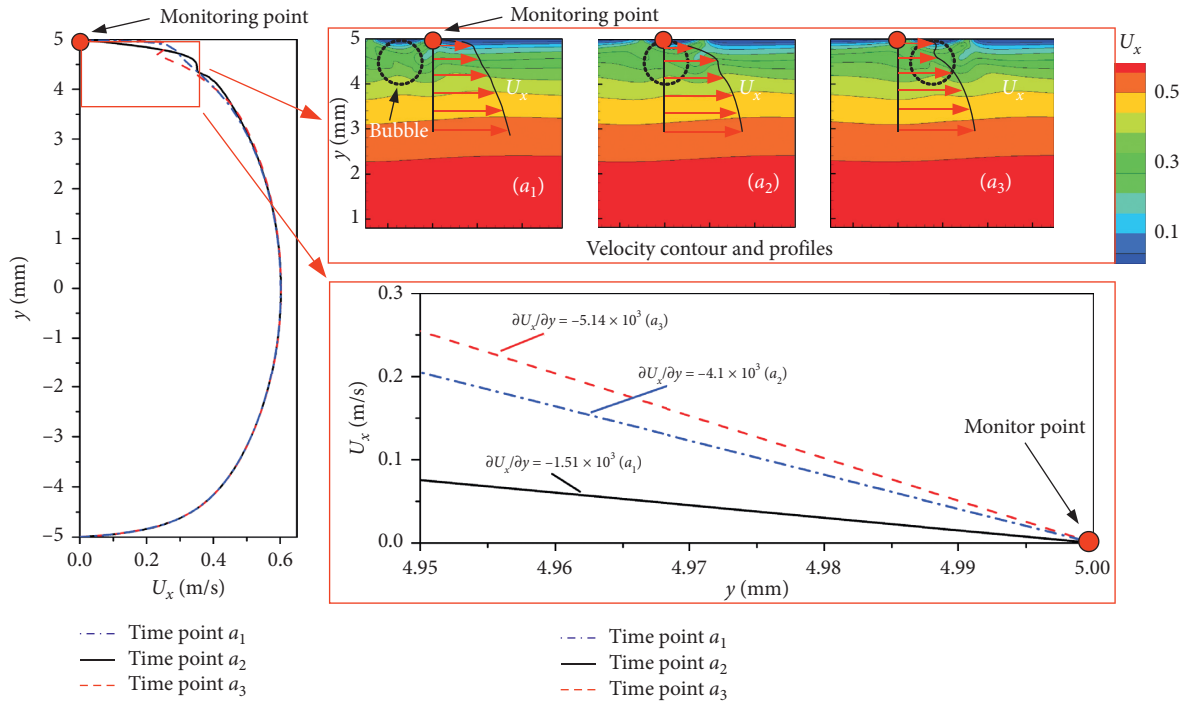
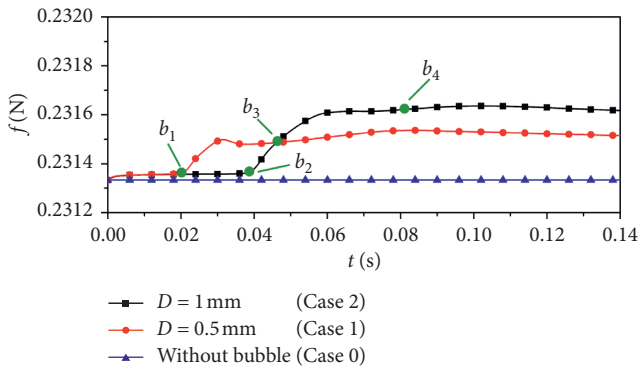FIGURE 8: Detailed effects of a bubble on the velocity near the monitoring point.

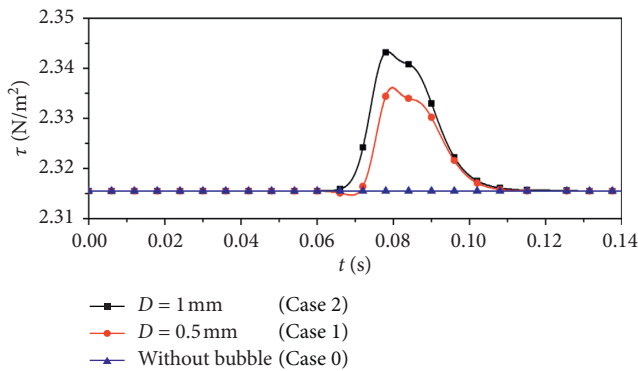FIGURE 9: Effects of bubble size on drag at the channel wall.

FIGURE 10: Effects of bubble size on the wall shear stress at the monitoring point.

FIGURE 11: Velocity distribution and profiles near the monitoring point.

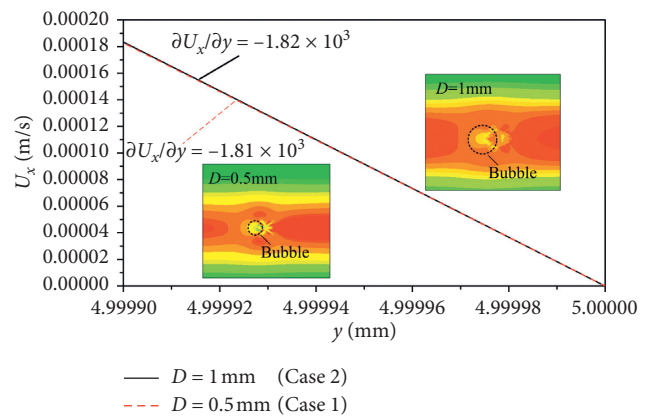bubble and two bubbles moving with water in the channel are conducted, corresponding to the case list in Table 1. For Case 2 and Cases 5 to 8 for a single bubble, as the distance of the bubble to the wall dh is lowered, and the interaction between the bubble and the wall is enhanced and leads to more significant perturbations of wall shear stress, as demonstrated in Figure 20. The wall shear stress at the monitoring point increases rapidly after reaching a low point and then decreases quickly to initial levels for Cases 5 to 8. Furthermore, the amplitude of the variation gradually increases when the distance of the bubble to the wall decreases. To uncover the interesting trend in this variation, Case 8 is chosen for further study due to its remarkable variation of wall shear stress.

To analyze the degree of influence of the velocity gradient at different bubble positions, nine typical time points from Case 8 are selected for discussion, as shown in Figure 21. The velocity distributions for different time points are shown in Figure 22. It is obvious that the velocity gradient has a maximum value at time point d_9 when the wall shear
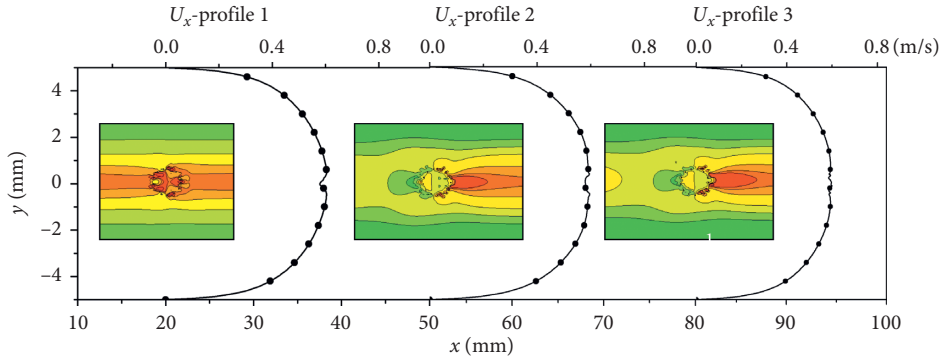
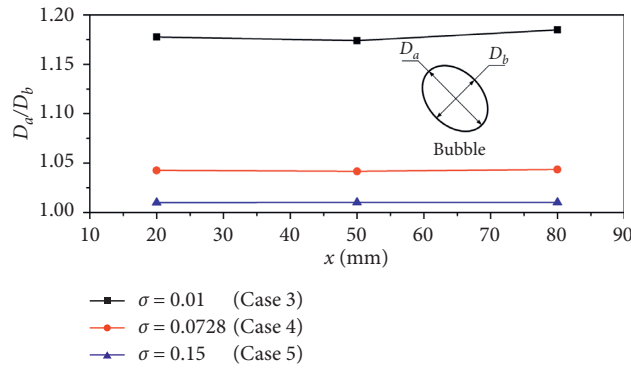FIGURE 12: Velocity profile changes caused by the bubble with $D = 1$ mm.

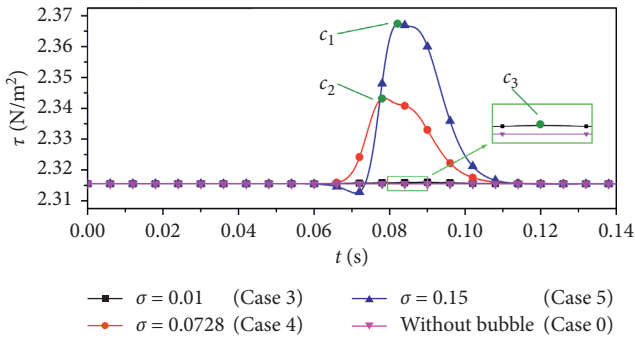FIGURE 13: Effects of surface tension on deformation of bubbles.

FIGURE 14: Effects of surface tension on the wall shear stress at the monitoring point.

FIGURE 15: Velocity distribution near the monitoring point.

stress reaches its peak value. Also, the gradient has a minimum value at time point d_7 when the shear wall stress reaches the valley. The reason for this situation is the fact that the bubble is located just below the monitoring point at time point d_7 as shown in Figure 23, and the flow structure is disturbed by the bubble so the velocity gradient is affected near the monitoring point. Briefly, the trends of the velocity gradients and wall shear stresses are similar. Furthermore, as the distance between the bubble and the wall decreases, drag at the wall increases, as shown in Table 1. In addition, it is clear that the turbulent kinetic energy around the bubble is bigger than those at other positions for Case 2 and Cases 5 to 8 as shown in Figure 24. The change of turbulent kinetic energy supports the trends of wall shear stress as well.
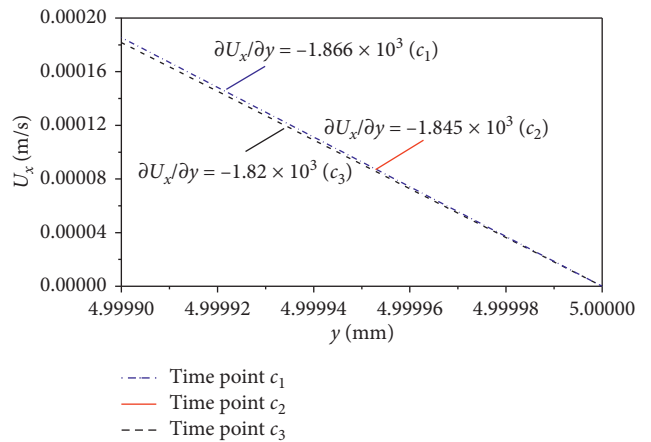
3.5. Effects of Bubbles' Initial Arrangement.

To investigate the effect of the bubbles' initial arrangement on the flow characteristics, numerical simulation are conducted with two bubbles arranged with the same distance of 2.5 mm vertically (Case 11) and horizontally (Case 10) respectively. The wall shear stresses at the monitoring point show obvious fluctuations, and several time points are selected to analyze the cause of this interesting phenomenon as shown in Figure 25. For Case 11, the wall shear stress at the monitoring point has two peak values and reaches a minimum value at timepoint e_3 (Figure 25). The reason for this phenomenon is the fact that the velocity profile in the y direction
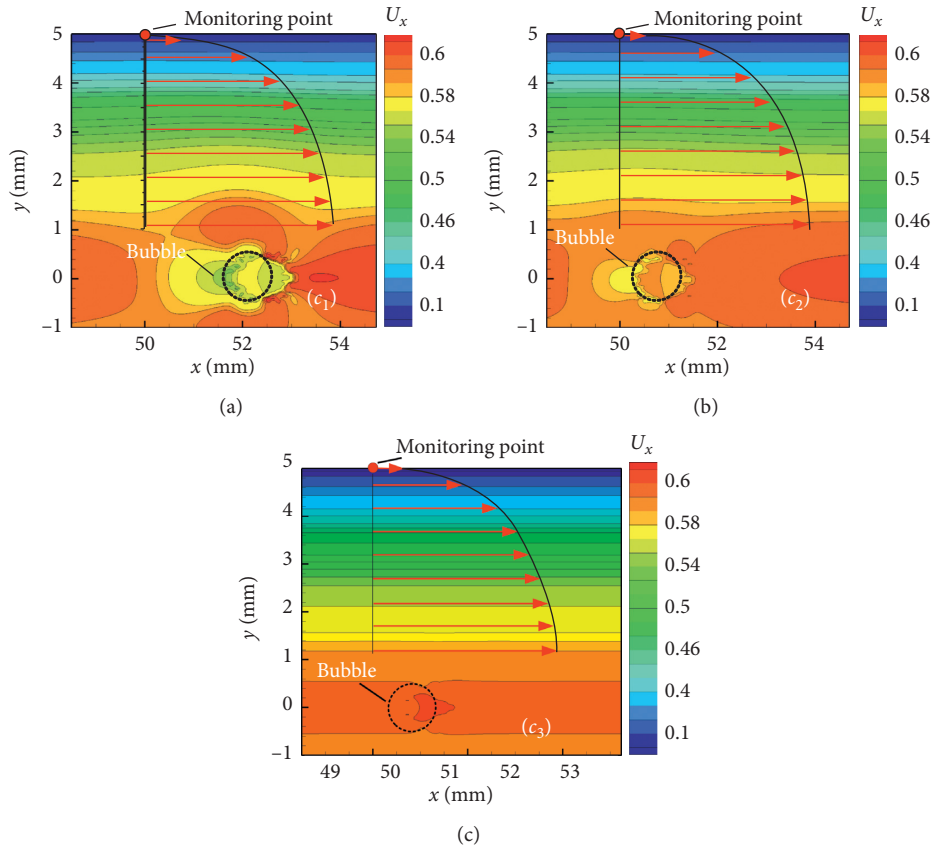
(a)

(b)

(c)

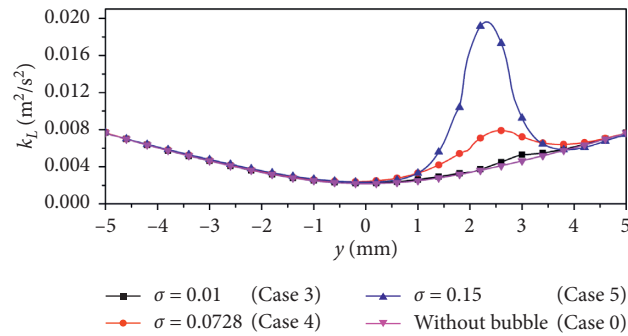Figure 16: Velocity contour and profiles near the monitoring point.

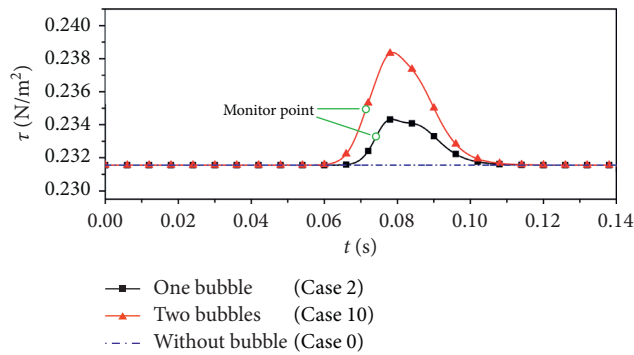Figure 17: Distribution of turbulent kinetic energy.

Figure 18: Effects of bubbles number on the wall shear stress at the monitoring point.
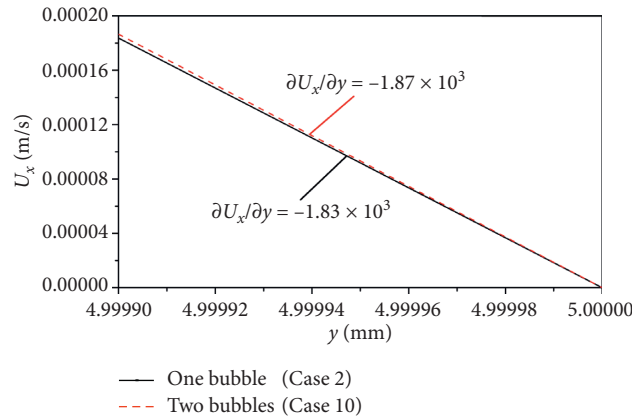
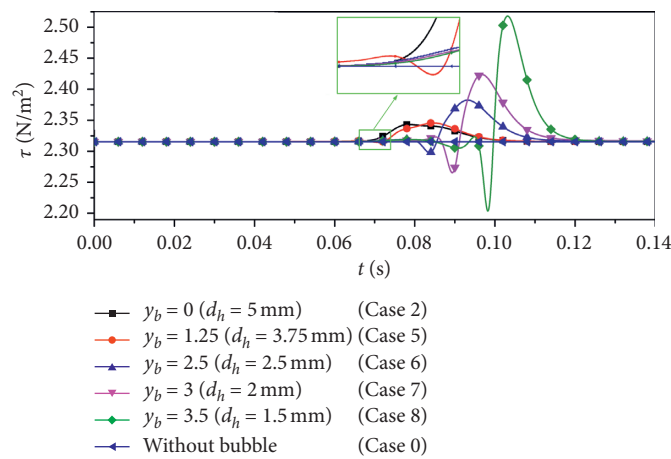Figure 19: Velocity distribution near the monitoring point.

Figure 20: Effects of bubble position (a single bubble) on wall shear stress at the monitoring point.
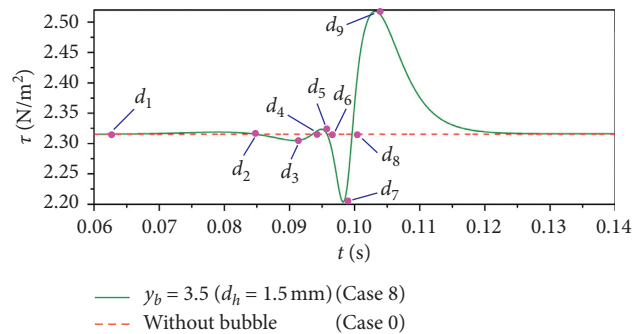

Figure 21: Positions of typical time points.

is non-uniform due to the existence of the wall boundary layer, resulting in a time difference when the two bubbles pass the monitoring point. As a result, the relative distance between the two bubbles in the x direction grows gradually (Figure 26). Compared with those at time points e_1 and e_3, the velocity gradients at the other three time points are much bigger, as shown in Figure 27. Furthermore, the velocity gradient at time point e_4 is slightly bigger than that at time point e_5, and both of them are distinctly bigger than that at time point e_2. This also explains the variation of wall shear stress and drag at the wall (Table 1) for Cases 10 and 11.

Flow characteristics near the monitoring point are applied to detail the above phenomena. The positions of bubbles at different time points and the velocity distribution near the monitoring point are shown in Figure 26. It is clear that bubble 1 has just passed the monitoring point at time point e_2, and at that time bubble 2 has not arrived yet. It takes time for the flow to respond to bubbles, and the velocity gradient fluctuation at the monitoring point at that time point is mainly affected by bubble 1. At time point e_3, the influence of the two bubbles is coincidentally neutralized, leading to little fluctuation of the wall shear stress. As shown
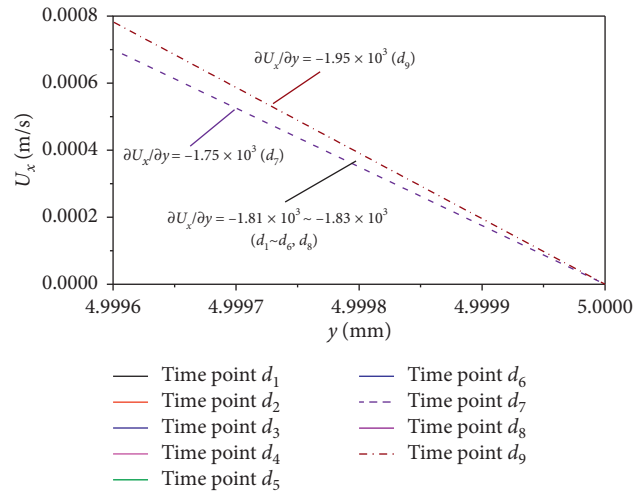
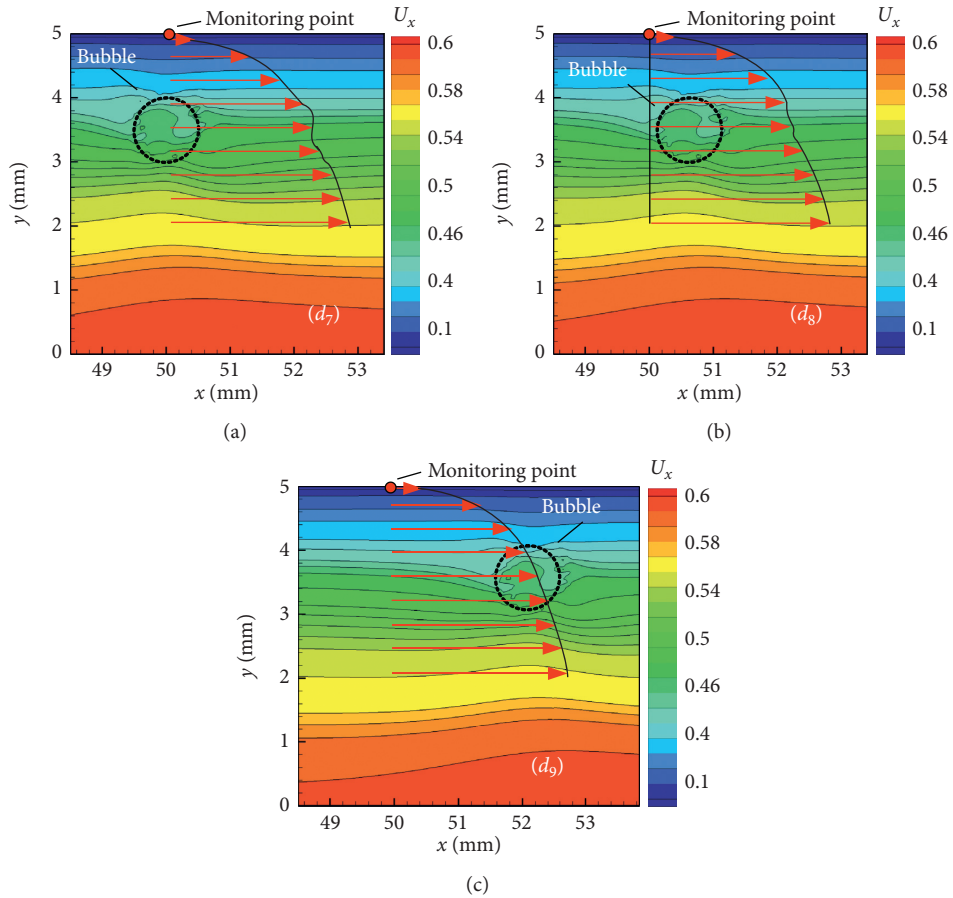FIGURE 22: Velocity distributions at different time points.

FIGURE 23: Velocity contour and profiles near monitoring point for different bubble positions.
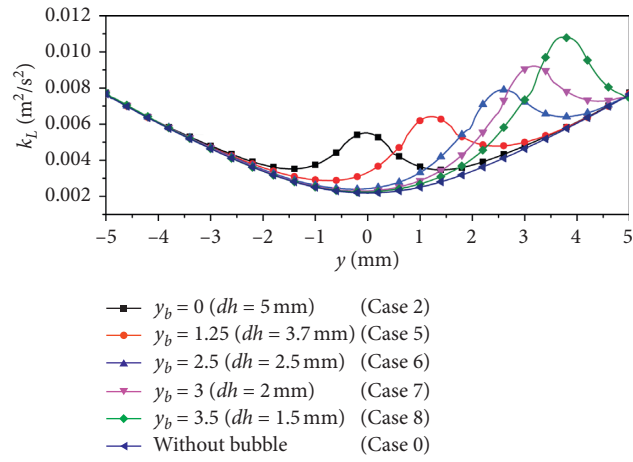
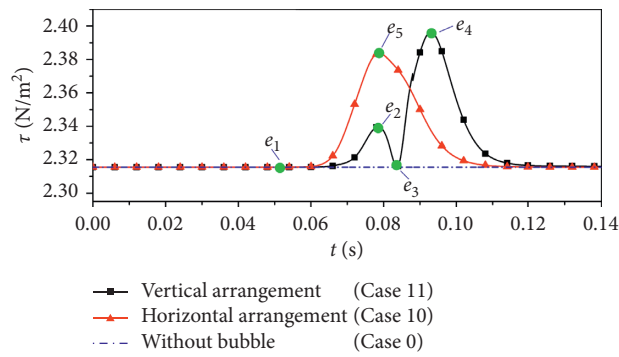FIGURE 24: Distribution of turbulent kinetic energy.

FIGURE 25: Effects of two bubbles' positions on wall shear stress at the monitoring point.

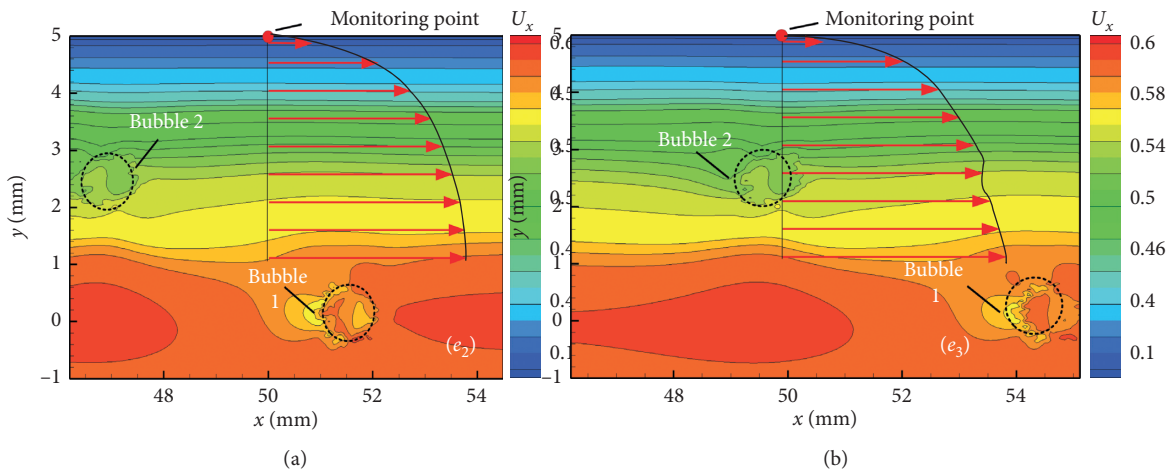(a)   (b)
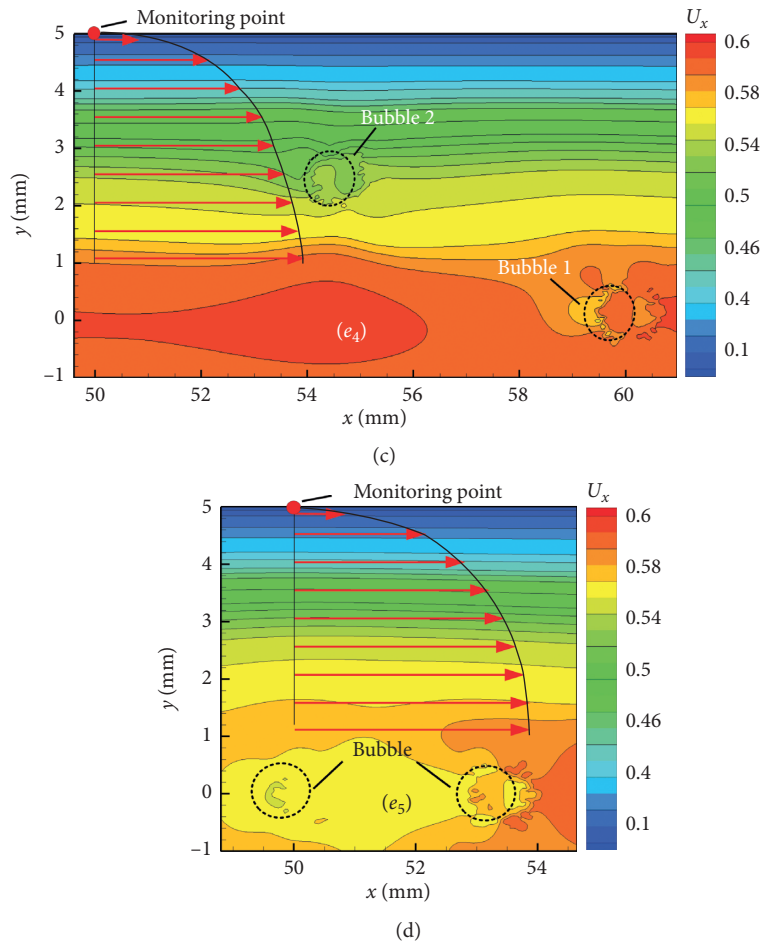
FIGURE 26: Continued.

(c)

(d)

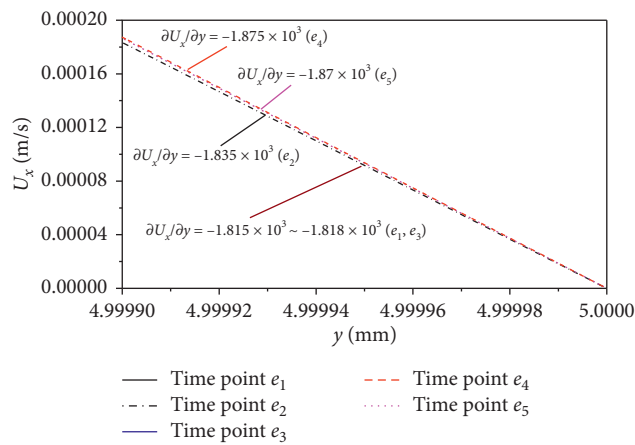Figure 26: Bubbly flow structure at different points in time.

Figure 27: Velocity profile at different time points near the monitoring point.

in Figure 26, at time point e_4, both bubbles have passed the monitoring point and bubble 2 dominates the influence on wall shear stress at the monitoring point. Since bubble 2 is closer to the wall, the wall shear stress at time point e_4 is much bigger than that at time point e_2. This phenomenon has been verified in Section 3.4 as well. For Case 10, the superposition of the influence of the two bubbles makes the peak shear stress value appear at time point e_5.

4. Conclusions

In this paper, the bubbly flow in a two-dimension channel is numerically investigated using ANSYS Fluent. The bubble-liquid interfaces are tracked with the VOF method, providing a way to clarify the bubble's effects on the flow structures and wall shear stresses under various bubble parameters such as bubble size, surface tension, bubbles number, initial positions of a single bubble and initial arrangements of multiple bubbles. Through the present investigation with CFD, the following conclusions can be drawn:

(1) The effect of larger bubbles on the drag at the wall is more significant than that of smaller ones, and both bubbles for the two cases result in a drag increase, in accordance with the studies summarized by Murai [7] as well.

(2) Higher bubble-liquid interfacial surface tension causes more drastic changes in wall shear stress and turbulent kinetic energy around the bubble, while lower surface tension causes a more pronounced deformation of the bubble and has little effect on the flow structures. Also, study of the effects of the bubble numbers reveals that more bubbles leads to greater influence on the wall shear stress.

(3) The change of turbulent kinetic energy reflects the trend of wall shear stresses. It is concluded that shorter distances between bubbles and the wall can enhance the flow interaction and lead to more significant flow perturbations due to effects from the bubbles from the wall shear stress and viscous drag.

Nomenclature

u: Velocity
μ: Viscosity of water
k: Turbulence kinetic energy
ε: Turbulence dissipation rate
G_b: Generation of turbulence kinetic energy due to buoyancy
Y_M: Contribution of the fluctuating dilatation to the overall dissipation rate
σ_k: Turbulent Prandtl numbers for k
σ_ε: Turbulent Prandtl numbers for ε
G_k: Generation of turbulence kinetic energy due to the mean velocity gradients
μ_t: Turbulent viscosity
α_q: Volume fraction
$\dot{m}$:   Mass transfer
ρ: Water density
Re: Reynolds number
h: Channel height
$U_{\max}$: The maximum of velocity along the x direction
τ: Wall shear stress.

Data Availability

Conflicts of Interest

The authors declare that they have no conflicts of interest.

Acknowledgments

References

[1] B. R. Elbing, E. S. Winkel, K. A. Lay, S. L. Ceccio, D. R. Dowling, and M. Perlin, "Bubble-induced skin-friction drag reduction and the abrupt transition to air-layer drag reduction," *Journal of Fluid Mechanics*, vol. 612, pp. 201–236, 2008.

[2] P. Baghaei, *Drag Reduction with the Aid of Air Bubbles and Additives*, University of Waterloo, Waterloo, Canada, 2009.

[3] H. Park, G. Sun, and C.-J. C. Kim, "Superhydrophobic turbulent drag reduction as a function of surface grating parameters," *Journal of Fluid Mechanics*, vol. 747, pp. 722–734, 2014.

[4] A. Slyozkin, M. Atlar, R. Sampson, and K.-C. Seo, "An experimental investigation into the hydrodynamic drag reduction of a flat plate using air-fed cavities," *Ocean Engineering*, vol. 76, pp. 105–120, 2014.

[5] S. A. Mäkiharju, M. Perlin, and S. L. Ceccio, "On the energy economics of air lubrication drag reduction," *International Journal of Naval Architecture and Ocean Engineering*, vol. 4, no. 4, pp. 412–422, 2012.

[6] S. L. Ceccio, "Friction drag reduction of external flows with bubble and gas injection," *Annual Review of Fluid Mechanics*, vol. 42, no. 1, pp. 183–203, 2010.

[7] Y. Murai, "Frictional drag reduction by bubble injection," *Experiments in Fluids*, vol. 55, Article ID 17737, 2014.

[8] E. Amromin, G. Karafiath, and B. Metcalf, "Ship drag reduction by air bottom ventilated cavitation in calm water and in waves," *Journal of Ship Research*, vol. 55, no. 3, pp. 196–207, 2011.

[9] K. Ouyang, S. Wu, and H. Huang, "Optimum parameter design of microbubble drag reduction in a turbulent flow by the Taguchi method combined with artificial neural networks," *Journal of Fluids Engineering*, vol. 135, no. 11, Article ID 111301, 2013.

[10] B. Jacob, A. Olivieri, M. Miozzi, E. F. Campana, and R. Piva, "Drag reduction by microbubbles in a turbulent boundary layer," *Physics of Fluids*, vol. 22, no. 11, Article ID 115104, 2010.

[11] I. Kumagai, Y. Takahashi, and Y. Murai, "Power-saving device for air bubble generation using a hydrofoil to reduce ship drag: theory, experiments, and application to ships," *Ocean Engineering*, vol. 95, pp. 183–194, 2015.

[12] S. Qin, N. Chu, Y. Yao, J. Liu, B. Huang, and D. Wu, "Streamwise distribution of skin-friction drag reduction on a flat plate with bubble injection," *Physics of Fluids*, vol. 29, no. 3, Article ID 37103, 2017.

[13] B.-G. Paik, G.-T. Yim, K.-Y. Kim, and K.-S. Kim, "The effects of microbubbles on skin friction in a turbulent boundary layer flow," *International Journal of Multiphase Flow*, vol. 80, pp. 164–175, 2016.

[14] R. A. Verschoof, R. C. A. van der Veen, C. Sun, and D. Lohse, "Bubble drag reduction requires large bubbles," *Physical Review Letters*, vol. 117, no. 10, Article ID 104502, 2016.

[15] S. Rawat, A. Chouippe, R. Zamansky, D. Legendre, and E. Climent, "Drag modulation in turbulent boundary layers subject to different bubble injection strategies," *Computers & Fluids*, vol. 178, pp. 73–87, 2019.

[16] X. Shen, S. L. Ceccio, and M. Perlin, "Influence of bubble size on micro-bubble drag reduction," *Experiments in Fluids*, vol. 41, no. 3, pp. 415–424, 2006.

[17] M. M. Peiravi, J. Alinejad, D. D. Ganji, and S. Maddah, "3D optimization of baffle arrangement in a multi-phase nanofluid natural convection based on numerical simulation," *International Journal of Numerical Methods for Heat & Fluid Flow*, vol. 30, no. 5, pp. 2583–2605, 2019.

[18] D. D. Ganji, M. M. Peiravi, and M. Abbasi, "Evaluation of the heat transfer rate increases in retention pools nuclear waste," *International Journal of Nano Dimension*, vol. 6, no. 4, p. 385, 2015.

[19] M. Sheikholeslami, M. Nimafar, and D. D. Ganji, "Nanofluid heat transfer between two pipes considering Brownian motion using AGM," *Alexandria Engineering Journal*, vol. 56, no. 2, pp. 277–283, 2017.

[20] J. Alinejad and M. M. Peiravi, "Numerical analysis of secondary droplets characteristics due to drop impacting on 3D cylinders considering dynamic contact angle," *Meccanica*, vol. 55, no. 10, pp. 1975–2002, 2020.

[21] M. M. Peiravi, J. Alinejad, A. D. Ganji et al., "Numerical study of fins arrangement and nanofluids effects on three-dimensional natural convection in the cubical enclosure," *Transport Phenomena in Nano and Micro Scales*, vol. 7, no. 2, pp. 97–112, 2019.

[22] M. M. Peiravi and J. Alinejad, "Hybrid conduction, convection and radiation heat transfer simulation in a channel with rectangular cylinder," *Journal of Thermal Analysis and Calorimetry*, vol. 140, no. 6, pp. 2733–2747, 2020.

[23] K. S. Asiagbe, M. Fairweather, D. O. Njobuenwu, and M. Colombo, "Large eddy simulation of microbubble transport in a turbulent horizontal channel flow," *International Journal of Multiphase Flow*, vol. 94, pp. 80–93, 2017.

[24] K. Mohanarangam, S. C. P. Cheung, J. Y. Tu, and L. Chen, "Numerical simulation of micro-bubble drag reduction using population balance model," *Ocean Engineering*, vol. 36, no. 11, pp. 863–872, 2009.

[25] M. J. Pang, J. J. Wei, and B. Yu, "Numerical study on modulation of microbubbles on turbulence frictional drag in a horizontal channel," *Ocean Engineering*, vol. 81, pp. 58–68, 2014.

[26] A. Ferrante and S. Elghobashi, "Reynolds number effect on drag reduction in a microbubble-laden spatially developing turbulent boundary layer," *Journal of Fluid Mechanics*, vol. 543, no. 1, p. 93, 2005.

[27] J. Xu, M. R. Maxey, and G. E. Karniadakis, "Numerical simulation of turbulent drag reduction using micro-bubbles," *Journal of Fluid Mechanics*, vol. 468, pp. 271–281, 2002.

[28] M. Pang and Z. Zhang, "Numerical investigation on turbulence drag reduction by small bubbles in horizontal channel with mixture model combined with population balance model," *Ocean Engineering*, vol. 162, pp. 80–97, 2018.

[29] J. Lu and G. Tryggvason, "Effect of bubble deformability in turbulent bubbly upflow in a vertical channel," *Physics of Fluids*, vol. 20, Article ID 040701, 2008.

[30] J. C. Lu, A. Fernandez, and G. Tryggvason, "The effect of bubbles on the wall drag in a turbulent channel flow," *Physics of Fluids*, vol. 17, Article ID 095102, 2005.

[31] X. Lyu, H. Tang, J. Sun, X. Wu, and X. Chen, "Simulation of microbubble resistance reduction on a suboff model," *Brodogradnja*, vol. 65, no. 2, pp. 23–32, 2014.

[32] J. L. G. Marinho, R. Swarnakar, S. R. de FariasNeto, and A. G. B. de Lima, "Unsteady fluidynamic behavior of gas bubbles flowing in curved pipes a numerical study," *Advances in Chemical Engineering and Science*, vol. 21, no. 2, pp. 283–291, 2012.

[33] R. O. Fox, "Large-eddy-simulation tools for multiphase flows," *Annual Review of Fluid Mechanics*, vol. 44, no. 1, pp. 47–76, 2012.

[34] T. H. Van Den Berg, D. P. Van Gils, D. P. Lathrop, and D. Lohse, "Bubbly turbulent drag reduction is a boundary layer effect," *Physical Review Letters*, vol. 98, no. 8, Article ID 84501, 2007.

[35] K. Mohanarangam, C. P. Cheung, J. Y. Tu, and L. Chen, "Skin friction reduction by introduction of micro-bubbles into turbulent boundary layer," in *Proceedings of the 16th Australasian Fluid Mechanics Conference*, Brisbane, Qld, Australia, December 2007.

[36] C. C. Gutierrez-Torres, Y. A. Hassan, and J. A. Jimenez-Bernal, "Turbulence structure modification and drag reduction by microbubble injections in a boundary layer channel flow," *Journal of Fluids Engineering*, vol. 130, no. 11, 2008.

[37] ANSYS, Inc., *ANSYS Fluent User's Manual*, ANSYS, Inc., Canonsburg, PA, USA, 2019.

[38] G. A. Whan and R. R. Rothfus, "Characteristics of transition flow between parallel plates," *AIChE Journal*, vol. 5, no. 2, pp. 204–208, 1959.